

RESEARCH ARTICLE

Magnetic resonance quantification of skeletal muscle lipid infiltration in a humanized mouse model of Duchenne muscular dystrophy

Ram B. Khattri^{1,2}  | Abhinandan Batra¹ | Michael Matheny³ | Cora Hart³ | Spencer C. Henley-Beasley³ | David Hammers³ | Huadong Zeng⁴ | Zoe White⁵ | Terence E. Ryan^{2,6} | Elisabeth Barton² | Pascal Bernatchez⁵ | Glenn A. Walter¹

¹Department of Physiology and Functional Genomics, University of Florida, Gainesville, Florida, USA

²Department of Applied Physiology and Kinesiology, University of Florida, Gainesville, Florida, USA

³Department of Pharmacology & Therapeutics, University of Florida, Gainesville, Florida, USA

⁴Advanced Magnetic Resonance Imaging and Spectroscopy Facility, University of Florida, Gainesville, Florida, USA

⁵Department of Anesthesiology, Pharmacology & Therapeutics, University of British Columbia, Canada

⁶Center of Exercise Science, University of Florida, Gainesville, Florida, USA

Correspondence

Glenn A. Walter, Department of Physiology and Functional Genomics, University of Florida, Gainesville, FL 32610, USA.
Email: glennw@ufl.edu

Funding information

Canadian Institutes of Health Research, and Senator Paul D. Wellstone Muscular Dystrophy Specialized Research Center (NIAMS: U54AR052646 and P50AR052646). National High Magnetic Field Laboratory, National Science Foundation Cooperative Agreement No. DMR-1644779 and the State of Florida. Pacific Airways Centre/Mitacs Accelerate fellowship.

Abstract

Rodent models of Duchenne muscular dystrophy (DMD) often do not recapitulate the severity of muscle wasting and resultant fibro-fatty infiltration observed in DMD patients. Having recently documented severe muscle wasting and fatty deposition in two preclinical models of muscular dystrophy (Dysferlin-null and *mdx* mice) through apolipoprotein E (*ApoE*) gene deletion without and with cholesterol-, triglyceride-rich Western diet supplementation, we sought to determine whether magnetic resonance imaging and spectroscopy (MRI and MRS, respectively) could be used to detect, characterize, and compare lipid deposition in *mdx-ApoE* knockout with *mdx* mice in a diet-dependent manner. MRI revealed that both *mdx* and *mdx-ApoE* mice exhibited elevated proton relaxation time constants (T_2) in their lower hindlimbs irrespective of diet, indicating both chronic muscle damage and fatty tissue deposition. The *mdx-ApoE* mice on a Western diet (*mdx-ApoE^W*) presented with greatest fatty tissue infiltration in the posterior compartment of the hindlimb compared with other groups, as detected by MRI/MRS. High-resolution magic angle spinning confirmed elevated lipid deposition in the posterior compartments of *mdx-ApoE^W* mice in vivo and ex vivo, respectively. In conclusion, the *mdx-ApoE^W* model recapitulates some of the extreme fatty tissue deposition observed clinically in DMD muscle but typically absent in *mdx* mice. This preclinical model will help facilitate the development of new imaging modalities directly relevant to the image contrast generated in DMD, and help to refine MR-based biomarkers and their relationship to tissue structure and disease progression.

KEYWORDS

Duchenne muscular dystrophy, fibro-fatty infiltration, magnetic resonance imaging and spectroscopy, mouse, muscle tissues, time domain nuclear magnetic resonance

Abbreviations used: AC, anterior compartment; ANOVA, analysis of variance; ApoE, apolipoprotein E; BMRB, Biological Magnetic Resonance Bank; DMD, Duchenne muscular dystrophy; gastroc, gastrocnemius; HR-MAS, high-resolution magic angle spinning; KO, knockout; MC, deep medial compartment; MD, muscular dystrophy; *mdx^W*, *mdx* mice on a Western diet; *mdx-ApoE^W*, *mdx-ApoE* mice on a Western diet; *mdx^R*, *mdx* mice on a regular diet; *mdx-ApoE^R*, *mdx-ApoE* mice on a regular diet; NOESY, nuclear Overhauser effect spectroscopy; PC, posterior compartment; PROJECT, periodic refocusing of J evolution by coherence transfer; STEAM, STimulated Echo Acquisition Mode; TDNMR, time domain nuclear magnetic resonance.

1 | INTRODUCTION

Animal models that reliably mimic and replicate the pathophysiological processes found in human diseases are crucial for the study of disease processes and the testing of therapeutic interventions. More than 60 different animal models have been generated and characterized in an attempt to better understand the muscle wasting and damage in Duchenne muscular dystrophy (DMD), the most common type of X-linked muscular dystrophy.¹ It is well established that myofiber damage, inflammation, and fibro-fatty infiltration are early hallmarks of this disease, which progresses to cardiac or respiratory failure by the second or third decade of life.²

Because of low costs and availability, the murine models of DMD have been the most extensively studied. One of the first dystrophin-deficient mice described is the *mdx* mouse, a spontaneous mutant with a premature stop codon in exon 23 of its *DMD* gene, leading to loss of dystrophin expression.³ Although the *mdx* mice model on the C57BL/10 background is widely studied, these mice present with a milder pathology and significant skeletal muscle hypertrophy attributable, in part, to enhanced regenerative capacities of murine muscle.⁴ By contrast, DMD patients show some degree of early compensatory hypertrophy, but this is followed by severe and irreversible muscle degeneration.² A number of strategies have been employed to generate mice more reflective of patients with DMD, including the hetero- and homozygotic ablation of utrophin in *mdx* mice⁵ (*mdx/utrophin* double mutant), genetic ablation of the *Cmah* gene (encoding cytidine monophosphate-sialic acid hydroxylase),⁶ backcrossing onto different mouse strains, and adoption of alternate mutations in dystrophin to prevent revertant fibers.^{7–10} While these strategies exacerbate muscle fragility and fibrosis, none of these models exhibit the overt fatty tissue replacement in muscles that characterizes DMD. To model these multiple dystrophic pathologies,¹¹ we used *mdx-4CV* mice, which have reduced revertant fibers, and inactivated their apolipoprotein E (*ApoE*) gene (*mdx-ApoE* mice), which predisposes the mice to heightened circulating cholesterol. These mice, when subjected to high-fat Western diet supplementation (*mdx-ApoE^W* mice),¹¹ have presented with elevated plasma lipid levels that are more representative of a human lipid profile.¹² Histological analyses of *mdx-ApoE* mice have revealed greater similarities with the human condition when compared with *mdx* mice retaining expression of *ApoE*. Because DMD may also be a new type of primary genetic dyslipidemia,¹³ modulating lipid levels in mice further enhances the similarity of human and rodent disease pathology.¹¹

MR imaging is a highly sensitive, noninvasive alternative for characterizing whole muscle wasting and additional pathological features associated with disease progression in DMD.^{14,15} The current study aimed to determine if *mdx-ApoE* mice recapitulated the MR biomarkers observed in DMD related to water T_2 and fatty tissue deposition. To achieve this, *mdx* and *mdx-ApoE* mice were fed either Western or normal chow diets and underwent MRI and in vivo MRS to quantify focal regions of fatty deposits in skeletal muscle. The results obtained were further validated ex vivo by quantifying fatty deposits in gastrocnemius (gastroc) muscle using high-resolution magic angle spinning (HR-MAS) $^1\text{H-NMR}$.

2 | MATERIALS AND METHODS

2.1 | Animals

The research was conducted according to the rules and guidelines provided by the Institutional Care and Use Committee, University of Florida, Gainesville, and the UBC Committee for Animal Care. Twenty-six *mdx* and *mdx-ApoE* mice were bred as previously described.¹¹ Nine mice (*mdx^R* [$n = 4$] and *mdx-ApoE^R* [$n = 5$]) were fed with regular Envigo 7917 chow diet (Madison, WI, USA), and 17 mice (*mdx^W* [$n = 8$] and *mdx-ApoE^W* [$n = 9$]) were fed a Western high-fat diet (Harlan, TD88137 consisting of 0.2% cholesterol, 21% total fat, and 34% sucrose by weight). Diets were started at the age of 8 weeks and continued until 32 weeks of age. Both male ($n = 19$) and female mice ($n = 7$) were utilized in this study. All imaging protocols and time domain nuclear magnetic resonance (TDNMR) were performed at 32 weeks of age. Following imaging protocols, the mice were euthanized to extract muscles of interest for histology and HR-MAS.

2.2 | Time domain nuclear magnetic resonance

TDNMR was used to quantify whole-body fat and lean body mass in these mice. The body composition of conscious mice was determined via a LF90 Minispec TDNMR analyzer (Bruker, Spring, TX, USA). A Plexiglas sample holder (90 mm in diameter and 250 mm in length) equipped with ventilation holes was used to hold the mice. The sample holder containing the mouse was loaded into the 0.5-T magnet bore, and measures were acquired (in triplicate) with a total measurement time of about 2 min per mouse.

2.3 | MRI T₂

MRI T₂ was used to evaluate pathological changes in muscles of the hindlimb, and was acquired on a 4.7-T (Agilent, Santa Clara, CA, USA) magnet system as previously described.¹⁶ Animals were anesthetized during MR scanning using isoflurane (3% induction, 0.75%–1% maintenance). The respiratory rate and temperature were continuously monitored during the scanning period to ensure the maintenance of anesthesia, and a heating system with flexible water pads was used to keep the animals warm during the scans. A custom-built 200-MHz ¹H solenoid coil with 1.5 cm internal diameter was used to image both hindlimbs together.

Proton T₂-weighted spin-echo images were acquired for lower hindlimb muscles (repetition time [TR]: 2000 ms; echo time [TE]: 14 and 40 ms; field of view: 10–15 mm × 10–15 mm; slices: 12; slice thickness: 1 mm; acquisition matrix: 256 × 128). Regions of interest (ROIs) representing muscle groups in the posterior compartment (PC), anterior compartment (AC), and deep medial compartment (MC) were manually traced over 5–8 slices using Horos (Horos is a free and open source code software program that is distributed free of charge under the LGPL license at Horosproject.org and sponsored by Nimble Co LLC d/b/a Purview in Annapolis, MD, USA) to calculate signal intensity. T₂ was calculated assuming a single exponential and two echoes as previously described.^{17,18}

2.4 | Magnetic resonance muscle spectroscopy

Magnetic resonance muscle spectroscopy was acquired on a 11.1-T MR horizontal bore magnet (Bruker Biospin, MA, USA) using a single-voxel ¹H-MRS STimulated Echo Acquisition Mode (STEAM) sequence localized to the PC (nominally the gastroc/plantaris complex). The localized pulse sequence was single-voxel STEAM^{19–21} with acquisition time (at) = 0.34 s, TR = 2 s, TE = 5 ms, spectral width (sw) = 6009.6 Hz, number of signal averages (NSA) = 256, voxel size = 2 × 2 × 2 mm³, and 2048 complex spectral datapoints with VAPOR for water suppression and outer-volume suppression. Water linewidths were in the range of 20–30 Hz. For consistency, STEAM spectra were acquired from a consistent region within all the mouse hindlimbs.

2.5 | ¹H high-resolution magic angle spinning NMR on ex vivo muscle tissue samples

¹H HR-MAS experiments were conducted with an 800-MHz Bruker spectrometer (Topspin 3.5p17 software) for intact gastroc tissue samples. The preparation of samples was performed following the protocols reported previously.^{22,23} Centralization of the tissue sample on the rotor was achieved by using a 3.2-mm inner diameter plastic insert that can confine about 50- μ l volume. Two sets of experiments—1D nuclear Overhauser effect spectroscopy (NOESY),^{24–28} and 1-D periodic refocusing of J evolution by coherence transfer (PROJECT) spectra²⁹ were conducted on each sample by spinning them with 5 KHz speed at 4°C, maintaining the magic angle of 54.7°. Both types of experiments were acquired using a 90-degree flip angle with sw = 6009.6 Hz and 256 scans. For the 1D NOESY spectra, a TR of 3.63 s was used (with a relaxation delay “d1” of 0.8 s and acquisition time [at] of 2.73 s) along with a mixing time of 100 ms.²³ The PROJECT spectra were collected with a TR of 3.53 s with 32 loops (L4).

2.6 | Chemical shift-encoded imaging

Chemical shift imaging sequences were used to perform fat water imaging. A standard multislice gradient echo imaging sequence (Bruker/FLASH) was acquired with individual TEs (1.8, 2.0, 2.5, 3.0, 4.0 ms), flip angle = 30, FOV = 15.0 × 15.0 mm², matrix = 192 × 192, TR = 200 ms, NSA = 4, slice thickness = 0.7 mm, sw = 150 KHz, and 16 slices. Fat and water maps were calculated using the MatLab toolbox³⁰ with a multiplex model reported in Triplett et al.³¹ after adjusting the frequencies for different magnetic field strengths.

2.7 | Muscle histology

Hindlimb muscles were harvested within 24 hr of imaging for histology and HR-MAS. Muscles were extracted and embedded in TissueTek OCT compound (Sakura Finetek, Torrance, CA, USA) and frozen using isopentane chilled in liquid nitrogen for histology. Frozen sections (8–10- μ m thick) were obtained from the midbelly region of gastroc muscle using a cryostat (Leica Microsystems, Solms, Germany). Multiple sections were taken and kept at room temperature for 20 to 30 min before staining them with H&E working solution.³²

2.8 | Data processing and analysis

All the HR-MAS and in vivo spectra were processed on a MestReNova 14.0.1–23559 (Mestrelab Research, S.L., Santiago de Compostela, Spain). Before applying Fourier transformation, the spectra were phased, baseline-corrected (with Spline), and the exponential line was broadened to 0.5 Hz. These spectra were calibrated with a lactate quartet at 4.11 ppm. Integration areas for the selected peaks were used to generate box and whisker plots using Prism (GraphPad Prism, version 8.4.2 for Windows, GraphPad Software, San Diego, CA, USA; www.graphpad.com). For the HR-MAS spectra, muscle wet weight correction was performed before carrying out any analysis. Assignment of the metabolites was performed as recommended in the literature^{12,33–35} and Biological Magnetic Resonance Bank (BMRB) data.³⁶ Dixon reconstructions were performed on magnitude and phase images using the ISMRM fat-water toolbox.³⁰

2.9 | Statistical analysis

Two-way analysis of variance (ANOVA) followed by a Tukey's multiple comparison test was performed to determine the statistical significance between the normal and Western high-fat diet groups. A p value of 0.05 or less was considered significant (with $p \leq 0.05$ indicated by [*/+], $p < 0.01$ by [**/+], and $p < 0.001$ by [***/+]). The values are reported as the mean \pm standard deviation. An asterisk indicates significantly different than regular/high-fat diet within the same strain, a hash tag indicates significantly different than the other strain within the high-fat diet groups, and plus indicates significantly different than regular/high-fat diet of the other strain.

3 | RESULTS

3.1 | TDNMR

Whole-body TDNMR was performed on a subset of mice ($n = 21$). *ApoE* knockout (KO) mice on both diets presented with no significant difference in overall body weight (*mdx-ApoE^R* [37.6 ± 1.2 g; $n = 5$] and *mdx-ApoE^W* [38.32 ± 5.3 g; $n = 7$]). *Mdx^W* ($n = 5$) presented with significantly higher body weight compared with *mdx^R* ($n = 4$). *Mdx^W* showed an increase in overall percentage body fat and decreased percentage lean muscle mass compared with the other three groups (Figure 1). This increase in whole-body fat deposition contrasts with the overt fat deposition in the gastroc muscle, highlighting the regional deposition of intramuscular fat.

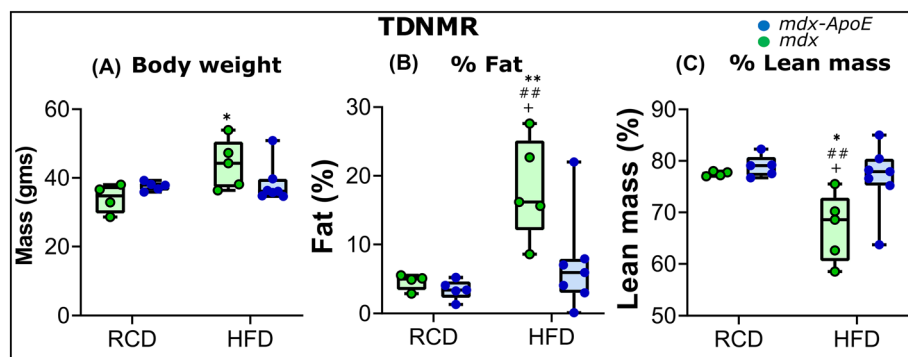


FIGURE 1 Box and whisker plots showing the (A) Body weight, (B) Fat percentage, and (C) Lean mass percentage of the mice among four different groups obtained from TDNMR. Significance was determined by two-way ANOVA with Tukey's multiple comparisons, and is considered significant if $p \leq 0.05$; $p \leq 0.05$ is denoted with */#/+; $p = 0.01–0.001$ is denoted with **/#/+; and $p \leq 0.001$ is denoted with ***/###/+++. Asterisk(s) mean significantly different within the same strain, the hash tag sign means significantly different than the other strain within the regular diet group, and the plus sign means significantly different than the HFD of the other strain. The number of samples per group were: *mdx-ApoE^R* ($n = 5$), *mdx-ApoE^W* ($n = 7$), *mdx^R* ($n = 4$), and *mdx^W* ($n = 5$). ANOVA, analysis of variance; HFD, high-fat diet; RCD, regular chow diet; TDNMR, time domain nuclear magnetic resonance

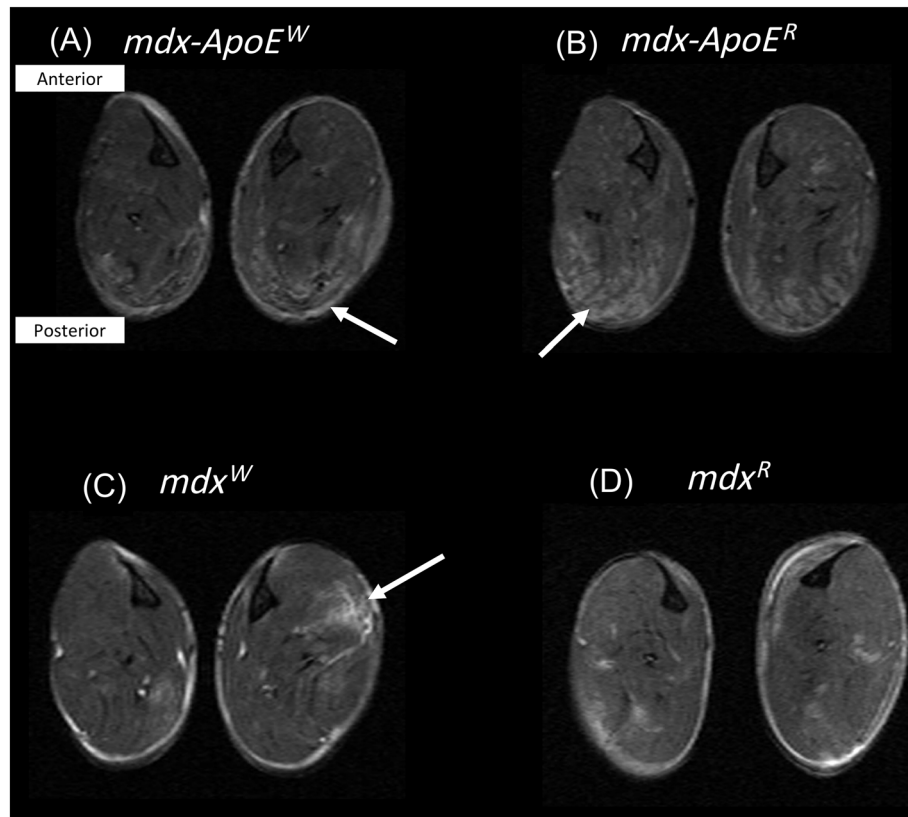


FIGURE 2 Representative T₂-weighted MRI images of *mdx* and *mdx-ApoE* mice on a Western high-fat diet or normal chow diet. (A) *mdx-ApoE^W*, (B) *mdx-ApoE^R*, (C) *mdx^W*, and (D) *mdx^R* groups. The number of samples per group were as follows: *mdx-ApoE^R* (n = 5), *mdx-ApoE^W* (n = 7), *mdx^R* (n = 3), and *mdx^W* (n = 5). Arrows indicate the areas of T₂ hyperintensity.

3.2 | T₂ measurement

MRI T₂ experiments were performed to visualize muscle damage in the lower hindlimb muscles. On visual examination of T₂-weighted images, hyperintense areas (depicted by arrows) were present in both the PC and the AC of all four groups of mice (Figure 2). On quantification, MRI T₂ from the PC (*mdx-ApoE^W* = 27.85 ± 1.8 ms; *mdx^R* = 25.96 ± 0.66 ms; *mdx-ApoE^R* = 25.55 ± 2.93 ms; *mdx^W* = 24.64 ± 1.11 ms) and the AC (*mdx-ApoE^W* = 25.0 ± 1.0 ms; *mdx^R* = 24.3 ± 0.3 ms; *mdx-ApoE^R* = 24.6 ± 2.6 ms; *mdx^W* = 24.9 ± 1.4 ms) was highest in *mdx-ApoE^W*, but was not significantly different in comparison with the other three groups.

3.3 | Lipid deposition in dystrophic muscle

In vivo proton spectra were acquired using single-voxel ¹H MRS localized to the PC (the gastroc/soleus/plantaris complex), as shown in Figure 3A–C. In comparison with the three other groups, *mdx-ApoE^W* presented with the highest lipid CH₂/creatinine ratio, a marker of myosteatosis³⁷ (Figure 3B). Lipid CH₂, which represents lipoproteins, showed a ~ 57- and 32-fold increase in *mdx-ApoE^W* compared with *mdx-ApoE^R* and *mdx^R*, respectively, and a ~ 22-fold increase compared with *mdx^W*. Further, the lipid CH₂/creatinine ratio in the *mdx-ApoE^W* group displayed a 66-, 37-, and 26-fold increase compared with the *mdx-ApoE^R*, *mdx^R*, and *mdx^W* groups, respectively. These findings suggest increased lipid infiltration of the muscles in the PC of hindlimbs of *mdx-ApoE* mice on a high fat diet.

3.4 | MRI: Chemical shift-encoded images

Clear areas of fat deposition were observed on fat fraction (FF) Dixon maps of lower hindlimb muscle in *mdx-ApoE^W* (Figure 4, top row; indicated by the arrow). This was further confirmed in the water maps, where a loss of signal can be appreciated in fat deposition areas (Figure 4, second row). Fatty deposition was present across multiple axial slices. Localized proton spectra from the PC further confirmed these findings showing

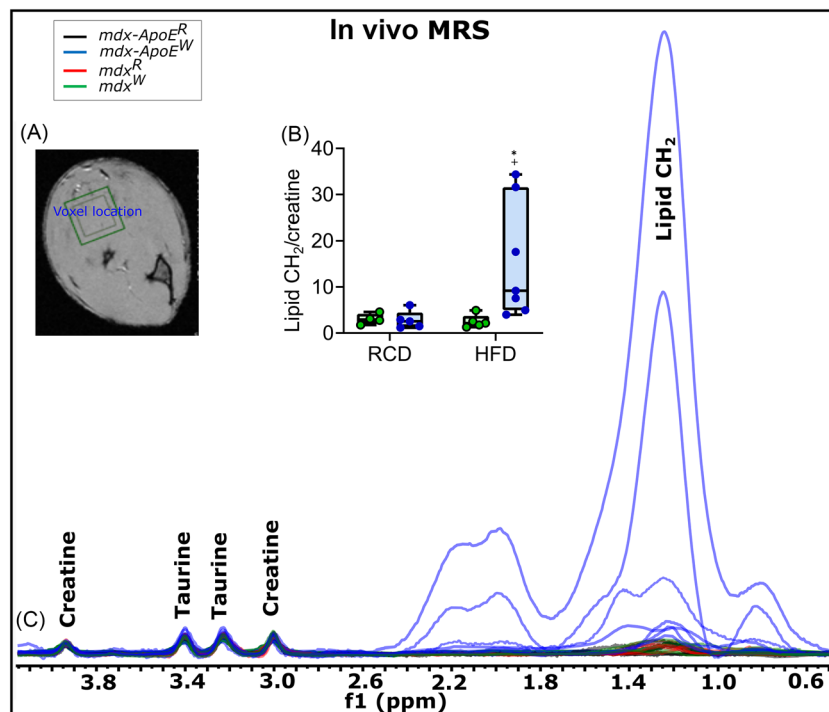


FIGURE 3 In vivo 1D ¹H spectra showing lipid CH₂, creatine, and taurine peaks. The lipid CH₂ level is elevated in the *mdx-ApoE^W* group. (A) The green square in the insert shows the location of the voxel utilized. (B) Box and whisker plot for lipid CH₂/creatinine, and (C) a portion of in vivo 1D ¹H spectra showing aliphatic regions. Significance was determined by two-way ANOVA with Tukey's multiple comparisons, and is considered significant if $p \leq 0.05$; $p \leq 0.05$ is denoted with */#/+; $p = 0.01-0.001$ is denoted with **/##/+++; and $p \leq 0.001$ is denoted with ***/###/++++. Asterisk(s) mean significantly different within the same strain, the hash tag sign means significantly different than the other strain within the regular diet group, and the plus sign means significantly different than the HFD of the other strain. The *mdx-ApoE^W* group was found statistically different than everybody else. The number of samples per group were: *mdx-ApoE^R* (n = 5), *mdx-ApoE^W* (n = 7), *mdx^R* (n = 4), and *mdx^W* (n = 5). All the spectra were normalized to the creatine resonance at 3.02 ppm. ANOVA, analysis of variance; HFD, high-fat diet; RCD, regular chow diet.

greater lipid content in the *mdx-ApoE* mice on a high-fat diet (*mdx-ApoE^W*) in comparison with the other three groups (Figure 4, right to the third row).

To quantify FF across different regions of the hindlimb, similar to T₂, manual ROIs were drawn around the posterior, medial, and anterior compartments. As was the case with T₂, there was a trend toward increased muscle FF in the PC of *mdx-ApoE^W*, but it was not significant (Figure 5).

3.5 | HR-MAS of gastrocnemius muscles

Based on the findings of in vivo results, ¹H HR-MAS spectra were acquired from the gastroc muscle ex vivo to further quantify metabolite changes in high-fat diet mice. A portion of ¹H HR-MAS spectra from the gastroc muscles capturing a subset of lipid and metabolite resonances are shown in Figure 6. High levels of lipids were clearly observed in the representative spectrum of the *mdx-ApoE^W* group (Figure 6A) compared with all the other groups, with the spectra from the *mdx^W* group (Figure 6D) displaying the second most prevalent lipid signature.

Of all the groups, lipid-CH₃ (integration of resonances from 0.83 to 0.96 ppm) and lipid-CH₂ (integration of resonances from 1.19 to 1.40 ppm) were significantly higher in *mdx-ApoE^W* (Figure 7A,B). Lipid-CH₃ was ~7-, ~18-, and ~4-fold higher in *mdx-ApoE^W* compared with the *mdx-ApoE^R*, *mdx^R*, and *mdx^W* groups, respectively. Similar findings were observed for -CH₂ resonances of fatty acids, unsaturated fatty acid (lipid -CH=CH-, integration of resonances from 5.27 to 5.42 ppm) and glyceryl moiety (resonances from 1.52 to 1.67 ppm and from 1.91 to 2.14 ppm for fatty acids, and from 4.22 to 4.35 ppm for glyceryl moiety) (Figure 7C-F). All the lipid classes mentioned above were significantly elevated in *mdx-ApoE^W* compared with the other groups (with p values ranging from 0.05 to 0.0001; Figure 7). These findings noninvasively confirm the histology findings from a previous study conducted by Milad et al., in which they found increased in oil red O staining in the gastroc muscle of *mdx-ApoE* KO mice.¹¹

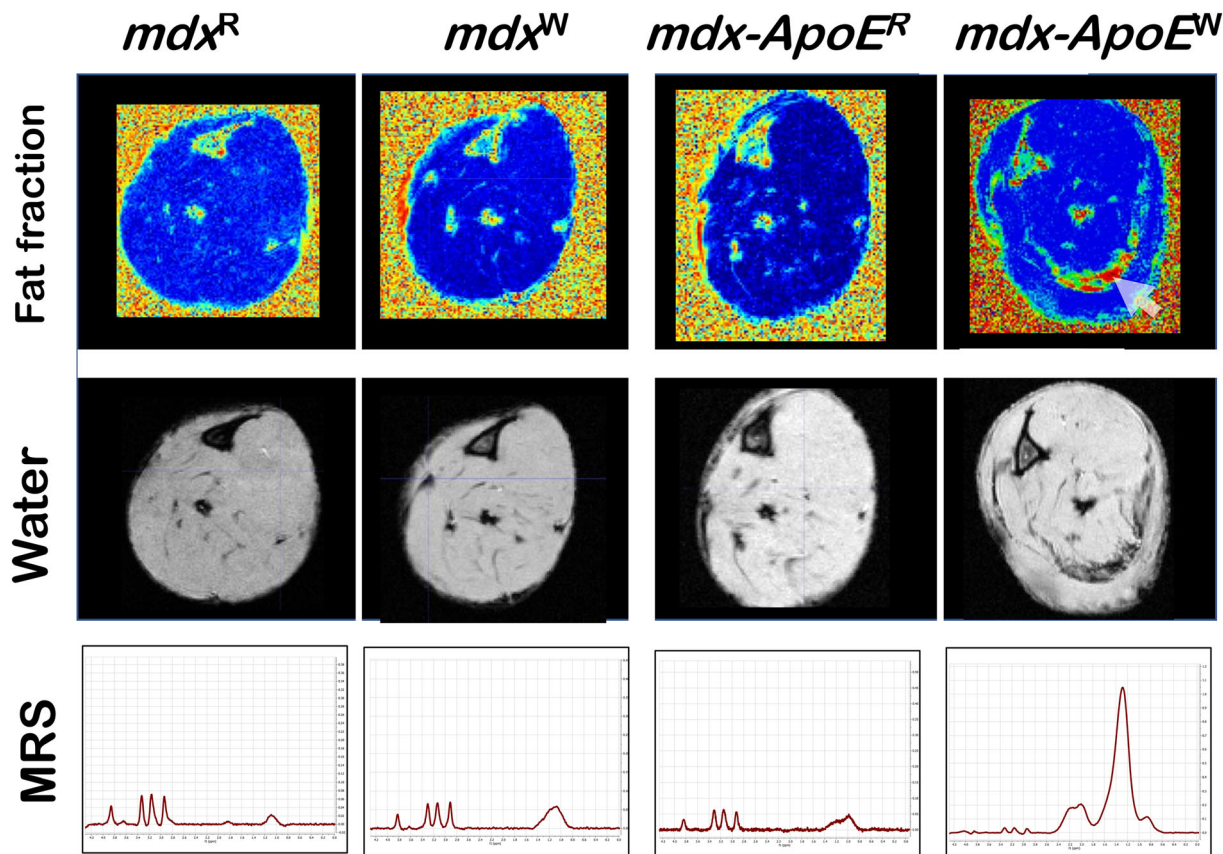


FIGURE 4 Representative chemical shift-encoded fat fraction and water maps (fat fraction: top row; water: second row) from the mdx^R , mdx^W , $mdx-ApoE^R$, and $mdx-ApoE^W$ groups. The white arrow in $mdx-ApoE^W$ indicates areas of fat deposits, which were visible on multiple images from each individual animal of that group. The third row shows the localized proton spectra, scaled to the total creatine resonance at 3.02 ppm, from the posterior compartment of each mouse.

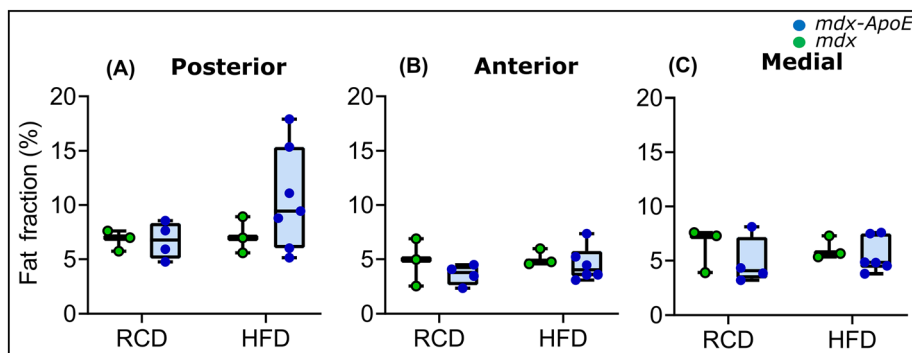


FIGURE 5 Box and whisker plots showing muscle fat fraction (%) in the entire posterior, anterior, and middle compartment of the lower hind-limb. (A) Fat fraction (%) in gastroc (posterior), (B) In TA (anterior), and (C) In MID (medial). Significance was determined by two-way ANOVA with Tukey's multiple comparisons, and is considered significant if $p \leq 0.05$; $p \leq 0.05$ is denoted with $*/\#/+$; $p = 0.01-0.001$ is denoted with $**/\#\#/+$; and $p \leq 0.001$ is denoted with $***/\#\#\#/+$. Asterisk(s) mean significantly different within the same strain, the hash tag sign means significantly different than the other strain within the regular diet group, and the plus sign means significantly different than the HFD of the other strain. The number of samples per group were as follows: $mdx-ApoE^R$ ($n = 4$), $mdx-ApoE^W$ ($n = 7$), mdx^R ($n = 3$), and mdx^W ($n = 3$). ANOVA, analysis of variance; gastroc, gastrocnemius; HFD, high-fat diet; RCD, regular chow diet; TA, tibialis anterior.

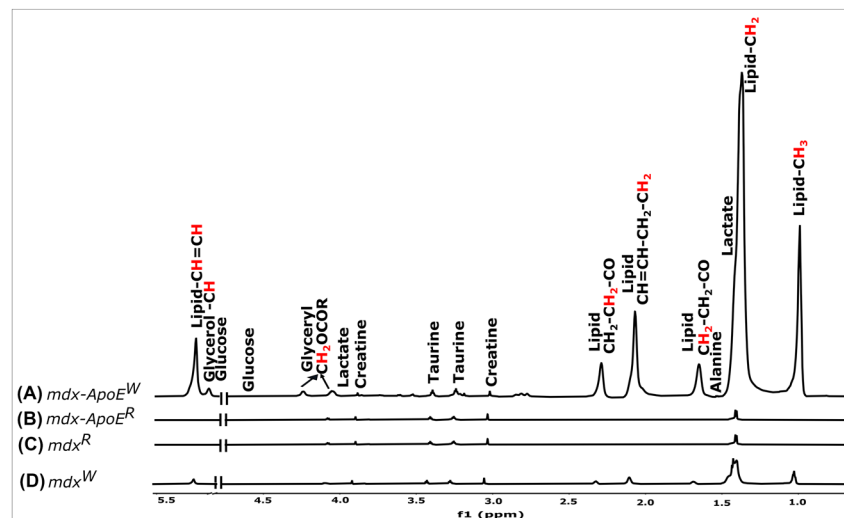


FIGURE 6 A portion of 1D ^1H HR-MAS representative spectra for gastrocnemius muscles showing some lipids and metabolite resonances. The elevation in lipid level can be clearly seen on Western high-fat diet samples. HR-MAS, high-resolution magic angle spinning.

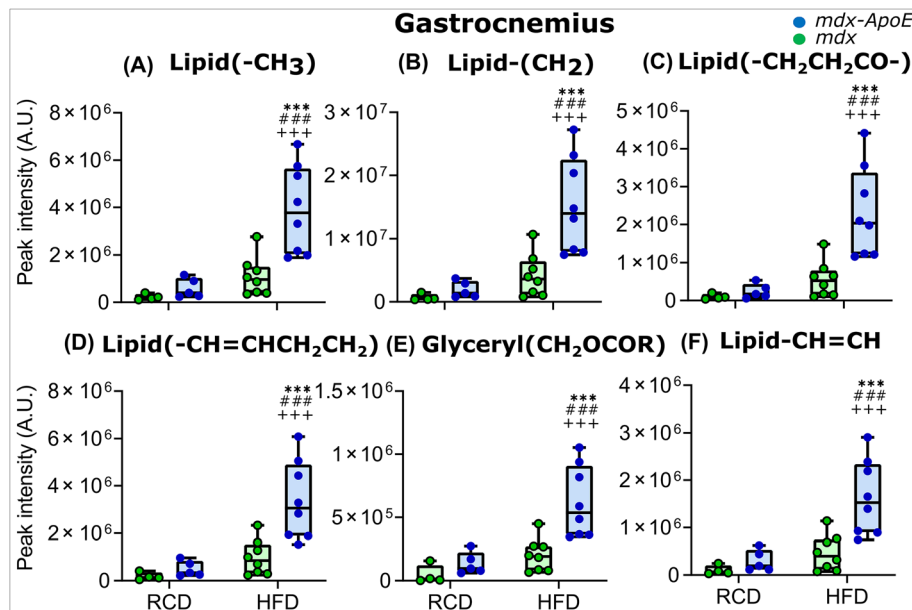


FIGURE 7 Box and whisker plots showing relative abundance of lipids for gastrocnemius samples via ^1H HR-MAS spectra. Significance was determined by two-way ANOVA with Tukey's multiple comparisons, and is considered significant if $p \leq 0.05$. $p \leq 0.05$ is denoted with $^*/\#/+$; $p = 0.01-0.001$ is denoted with $^{**}/\#\#/+$; and $p \leq 0.001$ is denoted with $^{***}/\#\#\#/+$. Asterisk(s) mean significantly different within the same strain, the hash tag sign means significantly different than the other strain within the regular diet group, and the plus sign means significantly different than the HFD of the other strain. The $mdx-ApoE^W$ group was found statistically different than other three groups. The number of samples per group were as follows: $mdx-ApoE^R$ ($n = 5$), $mdx-ApoE^W$ ($n = 8$), mdx^R ($n = 4$), and mdx^W ($n = 8$). ANOVA, analysis of variance; HFD, high-fat diet; HR-MAS, high-resolution magic angle spinning; RCD, regular chow diet

4 | DISCUSSION

In this study, we used a combination of different MR parameters to visualize and quantify lipid deposition in key muscles of a new preclinical model of DMD. Using the MRI proton relaxation time constant (T_2) and chemical shift-encoding imaging (also known as Dixon), we were able to visualize large areas of fatty tissue deposits in the muscles of $mdx-ApoE^W$, similar to what is observed in DMD.³⁸ Localized *in vivo* ^1H -MRS and ^1H HR-MAS of isolated gastroc muscles confirmed elevated fatty tissue infiltration in $mdx-ApoE^W$ mice compared with the other groups. We found that not only does the $mdx-ApoE^W$ model recapitulate many of the MRI characteristics of human DMD pathology, but it also provides a

preclinical dystrophic model in which noninvasive imaging methods of muscle damage and fatty tissue deposition can be tested and validated alongside histology (Supplementary Figure S1).

T_2 elevation has been shown to be associated with inflammation augmentation and lipid deposition in both preclinical¹⁶ and clinical DMD models.^{15,39} In this study, elevated T_2 was observed for the lower hindlimbs for all *mdx* models irrespective of diet, indicative of both chronic muscle damage and/or fatty tissue deposition in dystrophic muscle. Chemical shift-encoded MR images, in vivo ^1H -MRS, and ex vivo ^1H HR-MAS all confirmed that elevated MRI T_2 in *mdx-ApoE^W* was caused by increased fatty infiltration, as was evident through visual inspection of MR images and the higher percentage of fat in the PC of mice in this group. It is believed that in both DMD and in dystrophic *ApoE* KO mice, chronic rounds of muscle damage lead to replacement of muscle tissues with fat deposits.^{35,40}

Ex vivo ^1H HR-MAS showed increased fat infiltration in gastroc muscle for the *mdx-ApoE^W* group, supporting our in vivo and other MR findings. Several classes of lipids were significantly increasing in *mdx-ApoE^W*, indicating greater disease severity in this mice group.¹¹ A previous study performed by our group showed a greater extent of fat infiltration in the skeletal muscles of C57BL/10ScSn-DMD *mdx* mice compared with age-matched wild mice,⁴ and the fat infiltration was seen to be dramatically more exacerbated in the *mdx-ApoE^W* group used in this study compared with the previous study from our laboratory. Triglycerides were significantly elevated in the *mdx-ApoE^W* group, but we could not separate other classes of lipids such as cholesterol, phospholipids, phosphatidylcholines, lipoproteins, fatty acids, and their ester forms using ^1H HR-MAS for the gastroc tissue.⁴¹ The greater lipid accumulation in the gastroc muscle of *mdx-ApoE^W* crossvalidated the lipid deposition, as observed with Dixon imaging and elevated T_2 in the PC of hindlimbs in *mdx-ApoE^W* mice. In this study, we have only investigated gastroc muscle.

It is of interest to note that, compared with other well-known models of DMD, the *mdx-ApoE* mice seem to better mimic the disease severity of human DMD. In this study, we showed that the new *mdx-ApoE^W* mice recapitulate fat infiltration that is very similar to human DMD patients but that is typically absent in *mdx* mice. DMD affects the muscle in boys by replacing it with noncontractile and adipose tissue.¹² We believe that the new *mdx-ApoE^W* mouse model will help develop novel imaging modalities in preclinical models and refine biomarkers obtained via MR and, in turn, lead to more effective noninvasive evaluation of therapies targeting fatty infiltration.

Despite the fact that the current study relies on well-controlled mouse models of dystrophin deficiency and dyslipidemia, several limitations remain. For instance, factors such as diets, medications, surrounding environment, and genetic components can all contribute to dyslipidemia and muscle wasting in DMD patients⁴² and these were not investigated in this study. Another limitation is the absence of longitudinal measurements, and thus no critical conclusions can be drawn regarding the rate of age-related lipid infiltration in these muscles under study. The muscle heterogeneity is another factor that needs to be considered in future studies, because the rate of lipid infiltration may vary in the different muscle types. Because of the low-fat content and relatively high metabolite content (creatine, taurine, and choline) in the areas that lack fat infiltration, the spectral model used to separate fat from water using chemical shift-encoded MRI may be more complex than typically used in human muscle and/or liver, and thus warrants further investigation. The serum and HR-MAS data clearly show elevated lipid numbers; however, the inability to precisely localize the in vivo measures to the areas of the highest lipid deposition may have decreased the magnitude of the difference between the *mdx-ApoE^W* and the other groups because of partial volume contribution from muscle/muscle fibers with low fat content. Future studies focused on additional muscles known to show massive fatty tissue replacement in this mouse model (i.e., the triceps¹¹) and using a new high cholesterol diet⁴³ could increase the total volume of muscle lipid deposition and increase the potential for in vivo detection.

5 | CONCLUSIONS

Our findings suggest that noninvasive MRI along with MRS and HR-MAS spectroscopy are effective techniques with which to image and validate fat infiltration and lipid deposition in the hindlimbs of dystrophic mouse models. The hyperlipidemic *mdx-ApoE^W* model used in this study recapitulated many of the MRI biomarkers observed with DMD and can serve as a preclinical model for DMD and imaging biomarker development.

ACKNOWLEDGEMENTS

We would like to thank Dr. James Collins, Dr. Anil Mehta, James Rocca, and Professor Joanna Long, AMRIS, University of Florida, McKnight Brain Institute, Gainesville, FL, USA, for their help in completing this work. A portion of this work was supported by the National High Magnetic Field Laboratory, National Science Foundation Cooperative Agreement No. DMR-1644779 and the State of Florida. The major funding for this work came from the Canadian Institutes of Health Research, and Senator Paul D. Wellstone Muscular Dystrophy Specialized Research Center (NIAMS: U54AR052646 and P50AR052646). Dr. Zoe White is supported by a Pacific Airways Centre/Mitacs Accelerate fellowship.

CONFLICTS OF INTEREST

There are no conflicts to declare.

ORCID

Ram B. Khattri  <https://orcid.org/0000-0001-9991-263X>

REFERENCES

- McGreevy JW, Hakim CH, McIntosh MA, Duan D. Animal models of Duchenne muscular dystrophy: from basic mechanisms to gene therapy. *Dis Model Mech*. 2015;8(3):195-213. doi:10.1242/dmm.018424
- Townsend D, Yasuda S, Metzger J. Cardiomyopathy of Duchenne muscular dystrophy: pathogenesis and prospect of membrane sealants as a new therapeutic approach. *Expert Rev Cardiovasc Ther*. 2007;5(1):99-109. doi:10.1586/14779072.5.1.99
- Sicinski P, Geng Y, Ryder-Cook AS, Barnard EA, Darlison MG, Barnard PJ. The molecular basis of muscular dystrophy in the mdx mouse: a point mutation. *Science*. 1989;244(4912):1578-1580. doi:10.1126/science.2662404
- Lee-McMullen B, Chrzanowski SM, Vohra R, et al. Age-dependent changes in metabolite profile and lipid saturation in dystrophic mice. *NMR Biomed*. 2019;32(5):e4075. doi:10.1002/nbm.4075
- Deconinck AE, Rafael JA, Skinner JA, et al. Utrophin-dystrophin-deficient mice as a model for Duchenne muscular dystrophy. *Cell*. 1997;90(4):717-727. doi:10.1016/S0092-8674(00)80532-2
- Chandrasekharan K, Yoon JH, Xu Y, et al. A human-specific deletion in mouse Cmah increases disease severity in the mdx model of Duchenne muscular dystrophy. *Sci Transl Med*. 2010;2(42):42ra54.
- Calyjur PC, Almeida CF, Ayub-Guerrieri D, et al. The mdx mutation in the 129/Sv background results in a milder phenotype: transcriptome comparative analysis searching for the protective factors. *PLoS ONE*. 2016;11(3):e0150748. doi:10.1371/journal.pone.0150748
- Pillers DA, Weleber RG, Green DG, et al. Effects of dystrophin isoforms on signal transduction through neural retina: genotype-phenotype analysis of duchenne muscular dystrophy mouse mutants. *Mol Genet Metab*. 1999;66(2):100-110. doi:10.1006/mgme.1998.2784
- Pillers DA, Weleber RG, Woodward WR, Green DG, Chapman VM, Ray PN. mdxCv3 mouse is a model for electroretinography of Duchenne/Becker muscular dystrophy. *Invest Ophthalmol Vis Sci*. 1995;36(2):462-466.
- Coley W, Bogdanik L, Vila M, et al. Effect of genetic background on the dystrophic phenotype in mdx mice. *Hum Mol Genet*. 2016;25(1):130-145. doi:10.1093/hmg/ddv460
- Milad N, White Z, Tehrani AY, Sellers S, Rossi FMV, Bernatchez P. Increased plasma lipid levels exacerbate muscle pathology in the mdx mouse model of Duchenne muscular dystrophy. *Skelet Muscle*. 2017;7(1):19. doi:10.1186/s13395-017-0135-9
- Srivastava NK, Pradhan S, Mittal B, Gowda GA. High resolution NMR based analysis of serum lipids in Duchenne muscular dystrophy patients and its possible diagnostic significance. *NMR Biomed*. 2010;23(1):13-22. doi:10.1002/nbm.1419
- Amor F, Vu Hong A, Corre G, et al. Cholesterol metabolism is a potential therapeutic target in Duchenne muscular dystrophy. *J Cachexia Sarcopenia Muscle*. 2021;12(3):677-693. doi:10.1002/jcsm.12708
- Arpan I, Forbes SC, Lott DJ, et al. T₂ mapping provides multiple approaches for the characterization of muscle involvement in neuromuscular diseases: a cross-sectional study of lower leg muscles in 5-15-year-old boys with Duchenne muscular dystrophy. *NMR Biomed*. 2013;26(3):320-328. doi:10.1002/nbm.2851
- Forbes SC, Willcocks RJ, Triplett WT, et al. Magnetic resonance imaging and spectroscopy assessment of lower extremity skeletal muscles in boys with Duchenne muscular dystrophy: a multicenter cross sectional study. *PLoS ONE*. 2014;9(9):e106435. doi:10.1371/journal.pone.0106435
- Vohra RS, Mathur S, Bryant ND, Forbes SC, Vandenborne K, Walter GA. Age-related T2 changes in hindlimb muscles of mdx mice. *Muscle Nerve*. 2016;53(1):84-90. doi:10.1002/mus.24675
- Batra A, Vohra RS, Chrzanowski SM, et al. Effects of PDE5 inhibition on dystrophic muscle following an acute bout of downhill running and endurance training. *J Appl Physiol*. 2019;126(6):1737-1745. doi:10.1152/jappphysiol.00664.2018
- Mathur S, Vohra RS, Germain SA, et al. Changes in muscle T2 and tissue damage after downhill running in mdx mice. *Muscle Nerve*. 2011;43(6):878-886. doi:10.1002/mus.21986
- Fischer SE, Stuber M, Scheidegger MB, Boesiger P. Limitations of stimulated echo acquisition mode (STEAM) techniques in cardiac applications. *Magn Reson Med*. 1995;34(1):80-91. doi:10.1002/mrm.1910340113
- Gajdošik M, Chadzynski GL, Hangel G, et al. Ultrashort-TE stimulated echo acquisition mode (STEAM) improves the quantification of lipids and fatty acid chain unsaturation in the human liver at 7 T. *NMR Biomed*. 2015;28(10):1283-1293. doi:10.1002/nbm.3382
- Ibrahim E-S, Weiss RG, Stuber M, et al. Stimulated-echo acquisition mode (STEAM) MRI for black-blood delayed hyperenhanced myocardial imaging. *J Magn Reson Imaging*. 2008;27(1):229-238. doi:10.1002/jmri.21220
- Downes DP, Collins JHP, Lama B, et al. Characterization of brain metabolism by nuclear magnetic resonance. *ChemPhysChem*. 2019;20(2):216-230. doi:10.1002/cphc.201800917
- Khattri RB, Kim K, Thome T, et al. Unique metabolomic profile of skeletal muscle in chronic limb threatening ischemia. *J Clin Med*. 2021;10(3):548. doi:10.3390/jcm10030548
- Lohr KE, Khattri RB, Guingab-Cagmat J, et al. Metabolomic profiles differ among unique genotypes of a threatened Caribbean coral. *Sci Rep*. 2019;9(1):6067. doi:10.1038/s41598-019-42434-0
- Osis G, Webster K, Harris A, et al. Regulation of renal NaDC1 expression and citrate excretion by NBCe1-A. *Am J Physiol Renal Physiol*. 2019;317(2):F489-F501. doi:10.1152/ajprenal.00015.2019
- Ravanbakhsh S, Liu P, Björndahl TC, et al. Correction: Accurate, Fully-Automated NMR Spectral Profiling for Metabolomics. *PLoS ONE*. 2015;10(7):e0132873. doi:10.1371/journal.pone.0132873
- Myer C, Abdelrahman L, Banerjee S, et al. Aqueous humor metabolite profile of pseudoexfoliation glaucoma is distinctive. *Mol Omics*. 2020;16(5):425-435. doi:10.1039/C9MO00192A
- Myer C, Perez J, Abdelrahman L, et al. Differentiation of soluble aqueous humor metabolites in primary open angle glaucoma and controls. *Exp Eye Res*. 2020;194:108024. doi:10.1016/j.exer.2020.108024
- Le Guennec A, Tayyari F, Edison AS. Alternatives to Nuclear Overhauser Enhancement Spectroscopy Presat and Carr-Purcell-Meiboom-Gill Presat for NMR-Based Metabolomics. *Anal Chem*. 2017;89(17):8582-8588. doi:10.1021/acs.analchem.7b02354
- Hu HH, Börnert P, Hernando D, et al. ISMRM workshop on fat-water separation: insights, applications and progress in MRI. *Magn Reson Med*. 2012;68(2):378-388. doi:10.1002/mrm.24369
- Triplett WT, Baligand C, Forbes SC, et al. Chemical shift-based MRI to measure fat fractions in dystrophicskeletal muscle. *Magn Reson Med*. 2014;72(1):8-19.

32. Hammers DW, Hart CC, Matheny MK, et al. The D2.mdx mouse as a preclinical model of the skeletal muscle pathology associated with Duchenne muscular dystrophy. *Sci Rep*. 2020;10(1):14070. doi:[10.1038/s41598-020-70987-y](https://doi.org/10.1038/s41598-020-70987-y)
33. Srivastava NK, Pradhan S, Gowda GA, Kumar R. In vitro, high-resolution 1H and 31P NMR based analysis of the lipid components in the tissue, serum, and CSF of the patients with primary brain tumors: one possible diagnostic view. *NMR Biomed*. 2010;23(2):113-122. doi:[10.1002/nbm.1427](https://doi.org/10.1002/nbm.1427)
34. Srivastava NK, Annarao S, Sinha N. Metabolic status of patients with muscular dystrophy in early phase of the disease: In vitro, high resolution NMR spectroscopy based metabolomics analysis of serum. *Life Sci*. 2016;151:122-129. doi:[10.1016/j.lfs.2016.01.032](https://doi.org/10.1016/j.lfs.2016.01.032)
35. Srivastava NK, Yadav R, Mukherjee S, Pal L, Sinha N. Abnormal lipid metabolism in skeletal muscle tissue of patients with muscular dystrophy: In vitro, high-resolution NMR spectroscopy based observation in early phase of the disease. *Magn Reson Imaging*. 2017;38:163-173. doi:[10.1016/j.mri.2017.01.001](https://doi.org/10.1016/j.mri.2017.01.001)
36. Ulrich EL, Akutsu H, Doreleijers JF, et al. *Nucleic Acids Res*. 2008;36(Database issue):D402-408.
37. Wijsman CA, van Opstal AM, Kan HE, et al. Proton magnetic resonance spectroscopy shows lower intramyocellular lipid accumulation in middle-aged subjects predisposed to familial longevity. *Am J Physiol Endocrinol Metab*. 2012;302(3):E344-E348. doi:[10.1152/ajpendo.00455.2011](https://doi.org/10.1152/ajpendo.00455.2011)
38. Dunn J, Zaim-Wadghiri Y. Quantitative magnetic resonance imaging of the mdx mouse model of Duchenne muscular dystrophy. *Muscle Nerve*. 1999;22(10):1367-1371. doi:[10.1002/\(SICI\)1097-4598\(199910\)22:103.0.CO;2-H](https://doi.org/10.1002/(SICI)1097-4598(199910)22:103.0.CO;2-H)
39. Willcocks RJ, Arpan IA, Forbes SC, et al. Longitudinal measurements of MRI-T2 in boys with Duchenne muscular dystrophy: effects of age and disease progression. *Neuromuscul Disord*. 2014;24(5):393-401. doi:[10.1016/j.nmd.2013.12.012](https://doi.org/10.1016/j.nmd.2013.12.012)
40. Lott DJ, Forbes SC, Mathur S, et al. Assessment of intramuscular lipid and metabolites of the lower leg using magnetic resonance spectroscopy in boys with Duchenne muscular dystrophy. *Neuromuscul Disord*. 2014;24(7):574-582. doi:[10.1016/j.nmd.2014.03.013](https://doi.org/10.1016/j.nmd.2014.03.013)
41. Jiménez B, Holmes E, Heude C, et al. Quantitative Lipoprotein Subclass and Low Molecular Weight Metabolite Analysis in Human Serum and Plasma by. *Anal Chem*. 2018;90(20):11962-11971. doi:[10.1021/acs.analchem.8b02412](https://doi.org/10.1021/acs.analchem.8b02412)
42. White Z, Hakim CH, Theret M, et al. High prevalence of plasma lipid abnormalities in human and canine Duchenne and Becker muscular dystrophies depicts a new type of primary genetic dyslipidemia. *J Clin Lipidol*. 2020;14(4):459-469.e450. doi:[10.1016/j.jacl.2020.05.098](https://doi.org/10.1016/j.jacl.2020.05.098)
43. White Z, Theret M, Milad N, et al. Cholesterol absorption blocker ezetimibe prevents muscle wasting in severe dysferlin-deficient and mdx mice. *J Cachexia Sarcopenia Muscle*. 2022;13(1):544-560. doi:[10.1002/jcsm.12879](https://doi.org/10.1002/jcsm.12879)

SUPPORTING INFORMATION

Additional supporting information can be found online in the Supporting Information section at the end of this article.

How to cite this article: Khattri RB, Batra A, Matheny M, et al. Magnetic resonance quantification of skeletal muscle lipid infiltration in a humanized mouse model of Duchenne muscular dystrophy. *NMR in Biomedicine*. 2023;36(3):e4869. doi:[10.1002/nbm.4869](https://doi.org/10.1002/nbm.4869)